Direct observation of spin–orbit coupling in iron-based superconductors

S. V. Borisenko[1]*, D. V. Evtushinsky[1], Z.-H. Liu[1], I. Morozov[1,2], R. Kappenberger[1], S. Wurmehl[1,3], B. Büchner[1,3], A. N. Yaresko[4], T. K. Kim[5], M. Hoesch[5], T. Wolf[6] and N. D. Zhigadlo[7]

Spin–orbit coupling is a fundamental interaction in solids that can induce a broad range of unusual physical properties, from topologically non-trivial insulating states to unconventional pairing in superconductors[1-7]. In iron-based superconductors its role has, so far, not been considered of primary importance, with models based on spin- or orbital fluctuations pairing being used most widely[8-10]. Using angle-resolved photoemission spectroscopy, we directly observe a sizeable spin–orbit splitting in all the main members of the iron-based superconductors. We demonstrate that its impact on the low-energy electronic structure and details of the Fermi surface topology is stronger than that of possible nematic ordering[11-13]. The largest pairing gap is supported exactly by spin–orbit-coupling-induced Fermi surfaces, implying a direct relation between this interaction and the mechanism of high-temperature superconductivity.

In the presence of spin–orbit coupling (SOC), the electron's spin quantized along any fixed axis is no longer a good quantum number, but its total angular momentum is. This basic fact alone, or in combination with a particular symmetry breaking, may lead to a splitting of otherwise degenerate energy bands and is the origin of fascinating phenomena such as spin Hall effects[1], topological insulation[2], Majorana fermions[3] and so on. A special role has been played by SOC in the field of superconductors. In low-dimensional or noncentrosymmetric systems it can promote and stabilize superconductivity[4], allow ferromagnetism to coexist with superconductivity[5], or even raise T_c (ref. 6). It is anticipated that SOC could be a very important ingredient in describing the superconducting state in Sr_2RuO_4, where it is larger than the superconducting gap[7]. If SOC becomes sufficiently large, some materials can host topological superconductivity[3]. In iron-based superconductors (IBS), where the low-energy electronic states are composed of different orbitals, SOC-induced spin anisotropy together with the orbital mixing may directly influence the orbital and spin angular momentum of the Cooper pairs, thus making the determination of the pairing symmetry non-trivial. However, until now SOC in IBS was considered insignificant.

The reason may be understood from Fig. 1, where the results of the band-structure calculations are presented for the key members of the main families of iron pnictides and chalcogenides. A SOC-induced change of the electronic states at the low energies relevant for superconductivity is hardly seen. However, a number of recent ARPES experiments (for example, refs 14–17) have suggested a different picture, where the structures near the centre and the corners of the Brillouin zone (BZ) are apparently shifted in energy in opposite directions. The experimental Fermi level (horizontal red dashed lines) runs exactly through the regions with the multiple band extrema, resulting in small Fermi surfaces (FS), known to be important for superconductivity[18-20]. As is obvious from Fig. 1, SOC is expected to be significant in these regions.

To detect spin–orbit splitting and estimate its size in IBS, we start with the material where ARPES delivers the most exact spectral function. Because of stoichiometry, nonpolar surfaces, absence of structural or magnetic transitions, and considerable T_c, this material is LiFeAs (ref. 21).

There are several places where the effect of SOC on the band structure is large (Fig. 1, upper right panel). The best candidates situated close to the Fermi level, where the scattering is low and ARPES features are sharp, are the states near the Γ-point and near the experimental Fermi level crossing along the M–X direction. In both cases SOC qualitatively changes the band structure by splitting the bands which would be degenerate if SOC is absent. Figure 2 represents experimental data taken aiming at measurements of SOC at the Γ-point. To detect the possible splitting under the most suitable conditions, we have to locate the Γ-point in momentum space. If the in-plane location is defined by the normal emission, $k_z = 0$ can be found by recording the $k_x = k_y = 0$ spectrum as a function of photon energy. Such data, taken in the interval 20–110 eV with steps of 0.5 eV, are shown in Fig. 2a together with the results of the relativistic band-structure calculations along the Γ–Z direction (Fig. 2b, see also Fig. 1) using a false colour scale. Taking into account the renormalization factor of ~3 (ref. 21) and the square root dependence of k_z from the photon energy, the agreement is remarkable and even allows one to identify the strongly dispersing $3z^2 - r^2$ band with pronounced minima in the Z-points, which has not been detected previously. The Γ-points are located in between these well-defined Z-points and the corresponding photon energies can thus be easily found for both high-symmetry points. There are clearly two weakly dispersing features in the k_Z momentum regions near the Γ-points, as in the calculations. This is the first direct evidence of the presence of SOC in LiFeAs.

We show the photoemission intensity recorded along other high-symmetry directions, M–Γ–M and A–Z–A, together with the relativistic calculations in Fig. 2c,d and e,f respectively. Again, the experimental intensity distributions directly agree with the corresponding theoretical dispersions. Namely, all the dispersing features expected in calculations with SOC are present and their variations with k_Z are clearly seen. In particular, the tops of the two

[1]IFW-Dresden, Helmholtzstrasse 20, 01069 Dresden, Germany. [2]Lomonosov Moscow State University, GSP-1, Leninskie Gory, 119991 Moscow, Russian Federation. [3]Institute for Solid State Physics, TU Dresden, 01062 Dresden, Germany. [4]Max-Planck-Institute for Solid State Research, Heisenbergstrasse 1, 70569 Stuttgart, Germany. [5]Diamond Light Source, Harwell Campus, Didcot OX11 0DE, UK. [6]Institut für Festkörperphysik, Karlsruhe Institute for Technology, Karlsruhe 76021, Germany. [7]Laboratory for Solid State Physics, ETH Zurich, 8093 Zurich, Switzerland. *e-mail: S.Borisenko@ifw-dresden.de
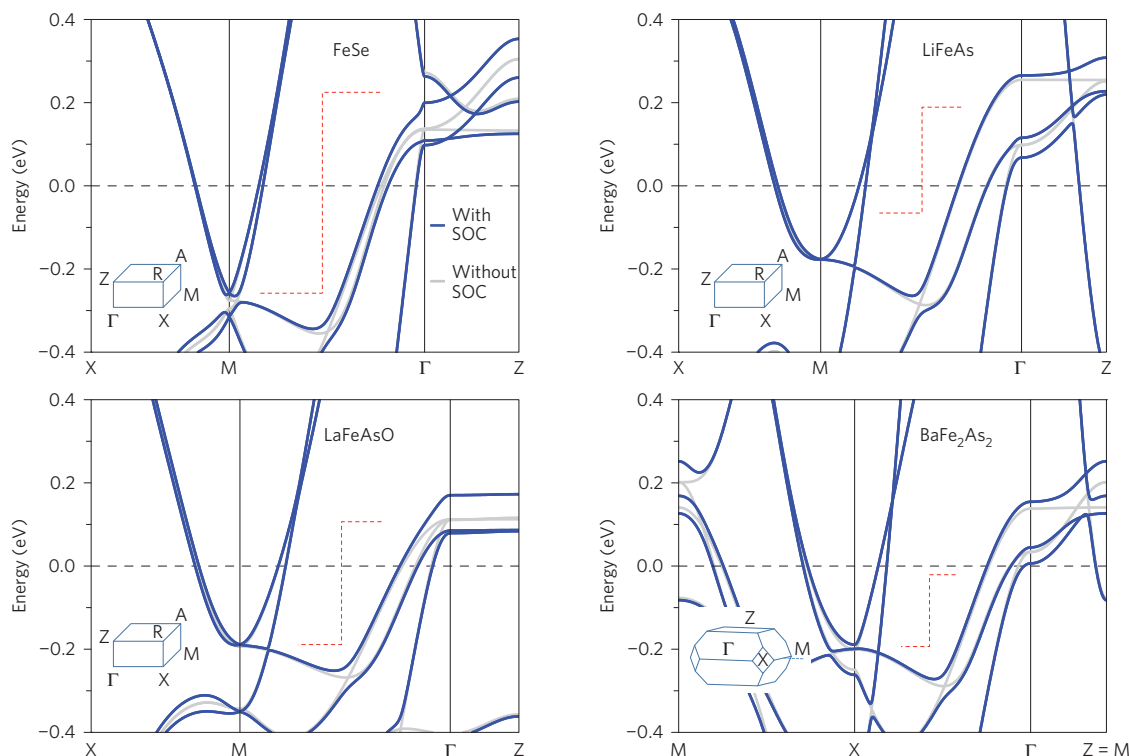
Figure 1 | Band-structure calculations of IBS with and without SOC. Electronic band dispersions of iron-based superconductors excluding SOC (grey lines) and including SOC (blue lines) along the high-symmetry directions. The corresponding Brillouin zones (BZ) with the high-symmetry points are shown in the insets. Horizontal red dashed lines correspond approximately to the experimental Fermi level in the ARPES measurements. Vertical red dashed lines separate the momentum regions in which the states are shifted in opposite directions in energy. Red dashed lines in the 122 IBS correspond to optimal hole doping with K.

parabolic bands are split and located below E_F in Fig. 2c, whereas one of them is above the Fermi level in Fig. 2e.

The value of SOC can now be directly read from the energy distribution curves (EDCs), corresponding to split parabolic bands at the Γ-points (Fig. 2g, upper panels). The average value of spin–orbit splitting is $\sim$10.7 meV, which is in agreement with the theoretical expectations, provided the renormalization is taken into account. In the lower panels of Fig. 2g we also show EDCs recorded in the superconducting state and using light of different polarization, as well as the single-peaked EDCs from the $k_F \sim 0.4\,\text{Å}^{-1}$. It is seen that the superconducting gap does not significantly influence the splitting by only slightly shifting the lower binding energy feature, which is not surprising because the maximum gap in LiFeAs is comparable to its energy position[22]. As expected, the opening of the gap has more impact on the k_F-EDCs, although the gap magnitude for this k_F is lower[22]. Polarization-dependent measurements confirm our assignment of the features to the spin–orbit split components: the lineshape of the EDC remains intact on switching to the vertical polarization (compare the upper and lower left panels of Fig. 2g), in sharp contrast to what is expected in the absence of orbital mixing due to SOC. If one of the features was of purely xz-character and the other of yz-character then their intensity ratio would strongly be sensitive to the switching of the light polarization. We stress here that it is not the lineshape of the EDCs alone that proves the presence of SOC, but rather the one-to-one correspondence between the experimental dispersing features recorded along the three high-symmetry directions and the relativistic band-structure calculations. It should be pointed out that similar lineshapes are also expected in the cases of strong coupling (for example, to a bosonic mode), but there two peaks arise from a single feature and an extended momentum region where such a lineshape remains constant typically exists. Here (Fig. 2c), we clearly

observe two continuous dispersions with separated tops—that is, strongly momentum-dependent splitting, as in the calculations.

Now we turn to another location in the k-space to measure the magnitude of the SOC on the electron pockets of LiFeAs. For this purpose we recorded the detailed Fermi surface map near the corner of the BZ (Fig. 3a) and the underlying dispersions (Fig. 3b,c). As follows from Fig. 3a, electron pockets are not degenerate along the M–X (A–R) direction, contrary to what one would expect from the non-relativistic band structure (Fig. 1). The energy splitting along the M–X direction is seen to be of the order of 10 meV, being slightly lower than that at the Γ-point (Fig. 2g), which is in close agreement with the renormalized calculated values. We have thus established the full correspondence between the experimental ARPES data from LiFeAs and relativistic band-structure calculations (Figs 1–3a–f) and experimentally determined the size of the maximal spin–orbit splitting ($\sim$11 meV) in this material.

Before switching to other IBS families, we have to establish to what degree another mechanism, nematicity, may contribute to the splitting at the centre of the BZ of LiFeAs, which has been suggested recently[23]. We do it with the help of a theoretical study[24] where the influence of both SOC and nematic effects, which lower the symmetry from tetragonal to orthorhombic, on the electronic structure is considered. According to this study, although the splitting at Γ-point can be a result of both effects, there should be a splitting of each of the bottoms of the electron pockets at the M-point if nematicity is present (Fig. 3g–i), whereas degeneracy of both bottoms is protected if only SOC is present (Fig. 3d–f). We will consider only the shallower pocket in LiFeAs, because the deeper pocket is broadened considerably by scattering (Fig. 3b,c). As follows from the experiment, there is no detectable splitting at the M-point. Moreover, the width of the corresponding EDC (see Supplementary Fig. 3c) is typical for this binding energy (that
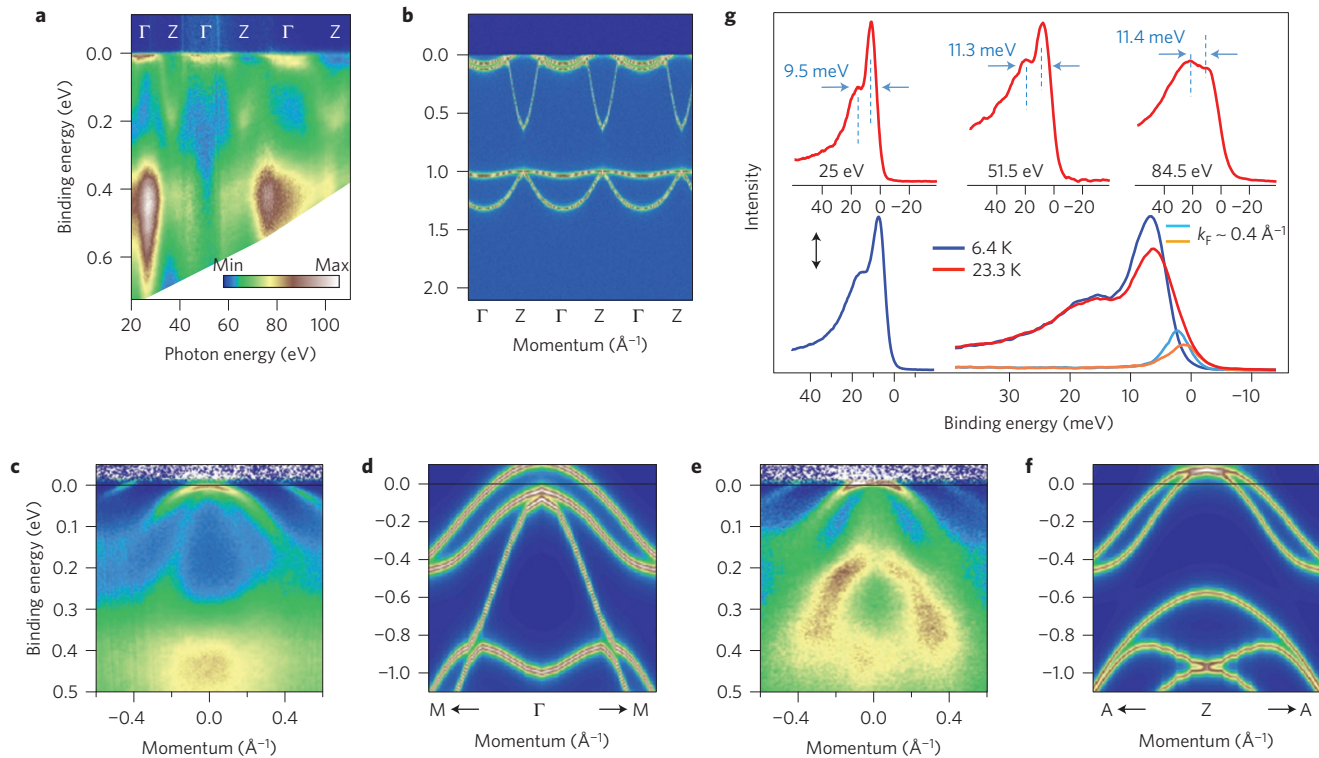
Figure 2 | Determination of spin–orbit splitting at Γ-point in LiFeAs. a, Photon-energy dependence of the normal emission EDC representing the band structure along the Γ–Z direction at $T = 23$ K. Hereafter, the 'terrain' false colour scale is the same for all intensity plots in the paper. **b**, Calculations with SOC along the Γ–Z direction for comparison with **a**. The false colour scale is used to indicate that more photoemission intensity is expected if, for example, two dispersions overlap. Calculated dispersions are broadened by a Gaussian. Hereafter, the zeroth binding energy in the calculations is shifted to match the experimental Fermi level. **c**, Energy–momentum intensity distribution recorded along the M–Γ–M direction at $T = 23$ K using 25 eV photons. **d**, Calculations with SOC for comparison with **c**. **e**, Same as **c**, but along the A–Z–A direction using 36.5 eV photons. **f**, Calculations with SOC for comparison with **e**. **g**, EDCs from the Γ-point taken at $T = 23$ K (red curves) and at $T = 6.4$ K (blue curves) using different photon energies and polarizations. Orange and light blue k_F-EDCs taken above and below T_c, respectively, are shown for comparison. Double-headed arrow in the lower left part indicates that this EDC is taken using vertically polarized light.

is, it is mostly defined by many-body effects), thus implying that the influence of nematic order cannot exceed a couple of meV. In addition, contributions from two domains would imply a doubling of all the dispersing features and corresponding FS (Fig. 3g–i), which is not seen experimentally. We have also checked that the splitting of the bottoms of the electron pockets is absent for different momenta along k_Z (see Supplementary Fig. 1e–p). Doping the LiFeAs with Co, as in all other IBS, results in broadening of the features because of the additional scattering on impurities, and detection of the SOC in those materials is therefore more difficult. For the sake of comparison with the results of ref. 23, we have recorded the EDC in the Γ-point of the 10%-doped compound and found a comparable value of SOC (see Supplementary Fig. 3f). The temperature does not influence the observed splitting in LiFeAs either (see Supplementary Fig. 1a,b). However, increasing temperatures to values comparable with the splitting would obviously hinder the observation of an ∼10 meV splitting of two features with intrinsic widths of ∼5 meV each, which would merge into a seemingly single broad peak[23].

The decisive evidence to support the dominant role of spin–orbit interaction in comparison with the nematic effects comes from similar experiments on FeSe, the simplest IBS, which exhibits the structural transition at 87 K and nematicity is expected to be more noticeable than in LiFeAs (refs 11–13). In Fig. 4a–f we show the spectra taken along cuts passing through the Γ-, Z- and M-points and compare them with the relativistic band-structure calculations (Fig. 1). There is a close qualitative correspondence between theory and experiment as far as the behaviour of the dispersing features is concerned, as in LiFeAs. The peculiar k_z dispersion of the states near

the Fermi level is strongly influenced by the presence of the $3z^2 - r^2$ band, and such an agreement with the experiment clearly implies its presence also in FeSe. The SOC in FeSe is predicted to be larger than in LiFeAs, as is immediately seen experimentally (∼25 meV in FeSe versus 11 meV in LiFeAs). If this larger splitting was due to nematic ordering effects, one would expect it to be clearly seen in the M-point. To minimize the complications connected with the presence of additional crossings stemming from another electron pocket and the possible influence of domains[11–13,24], we present the results taken along the M–X direction (compare Fig. 3e,h with Fig. 3f,i). As Fig. 4f shows, in FeSe one is able to track the behaviour of both shallow and deep electron pockets because both are located at lower binding energies than in LiFeAs (lower scattering). Again, in both cases the bottoms of the electron pockets seem to remain degenerate, contrary to what is expected if nematic splitting is strong (Fig. 3i). Here we can determine the upper limit of the possible nematic splitting. The corresponding EDC (see Supplementary Fig. 3b) has two peaks separated by ∼50 meV. Taking into account the intrinsic widths of these peaks, the possible remaining splitting of each of them, not detected because of finite energy resolution, is of the order of 5 meV. This is in agreement with the splitting expected due to the tetragonal-to-orthorhombic structural transition at 87 K in band-structure calculations (not shown). In addition, as in the case of LiFeAs, we do not see any doubling of the dispersion features because of the possible domains[24].

We also present the analogous data for other two main families of IBS. In Fig. 4g the spin–orbit splitting is clearly seen in overdoped Co-BaFe$_2$As$_2$ ($T_c \sim 10$ K), where it is possible to see both (originally
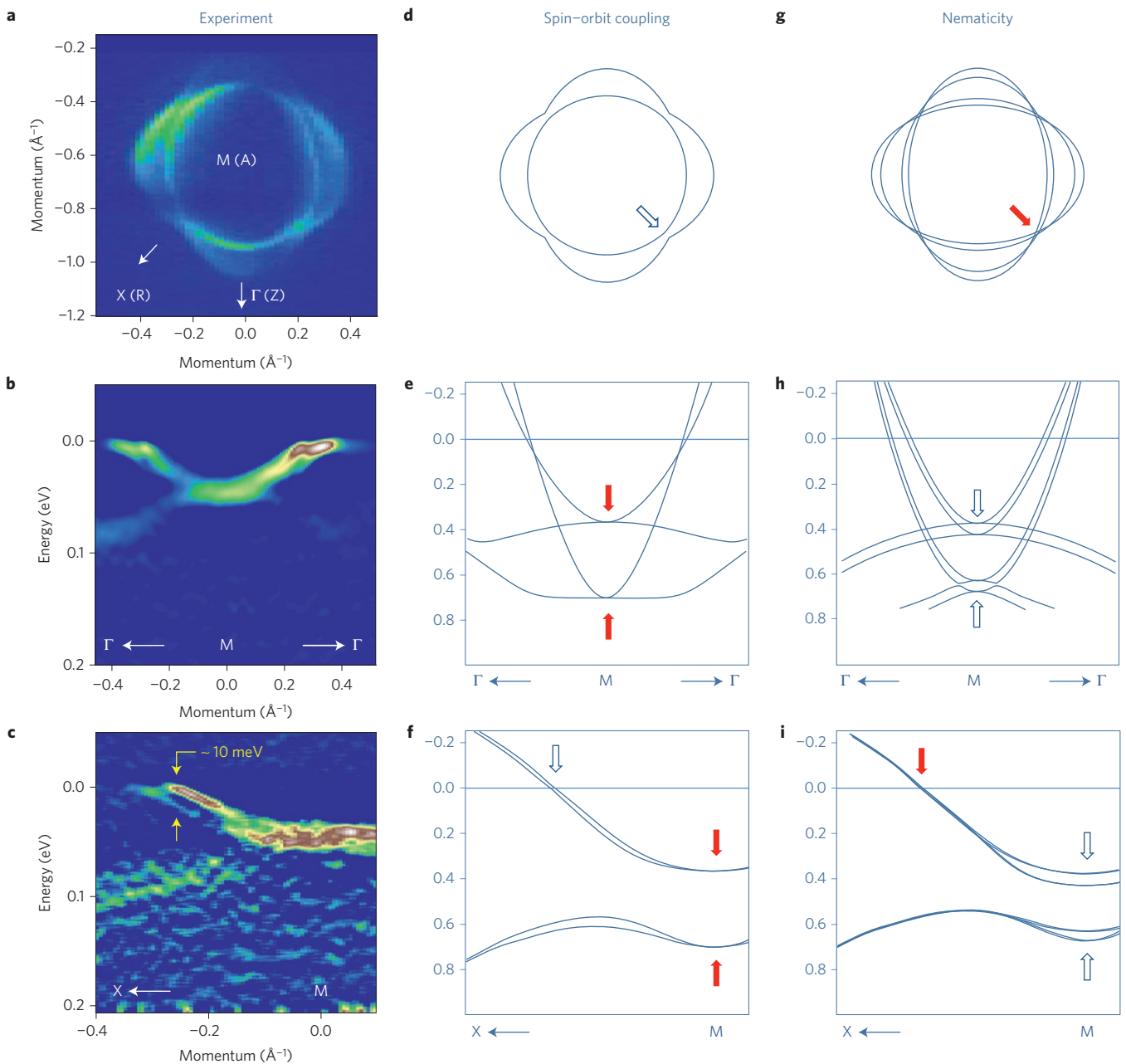
Figure 3 | Spin–orbit versus nematic splittings on electron-like pockets in LiFeAs. a, High-precision Fermi surface map of electron pockets in LiFeAs recorded at 23 K ($T > T_c$). White arrows show the direction to the high-symmetry points. **b,** Second derivative of the photoemission intensity plot showing the dispersions along the Γ–M–Γ direction. **c,** Same as **b,** but along the X–M–X direction. Raw data corresponding to **b** and **c** are shown in Supplementary Information (see Supplementary Fig. 1). **d–f,** Schematic representation of the calculations corresponding to the experimental data sets in the case when only spin–orbit interaction is taken into account. **g–i,** Same as **d–f,** but for the nematic scenario (adapted from ref. 24, not specific to LiFeAs). Hereafter, thick white (red) arrows indicate the splitting (degeneracy) of two features in energy or momentum.

xz and yz) bands below the Fermi level at the Γ-point. In the case of the optimally hole-doped 122 material ($T_c \sim 38$ K), there is no possibility of determining the SOC directly because the tops of all hole-like bands are well above the Fermi level, in accordance with lower electron concentration. We circumvent this limitation in the following way. As was found earlier[25], because of the sizeable superconducting gap and the proximity of the band's edges to E_F, the top of the band is 'reflected' to the occupied side of the spectrum below T_c, as schematically shown in Fig. 4h. The SOC can be then determined from the corresponding EDC (see Supplementary Fig. 3d). Another peculiarity of the 122 family is that the SOC should now lift the degeneracy in the corner of the BZ (now the

X-point, not the M-point, because the BZ is different) because of the different crystal structure (Fig. 1). This splitting is indeed seen experimentally (Fig. 4i). Finally, we detect the splitting in a representative of the 1111 family, Co-SmFeAsO ($T_c \sim 16$ K). In accordance with the calculations (Fig. 1), there is a splitting in the Γ-point and it is absent in the M-point (Fig. 4j,k). We summarize our observations in Fig. 4l, where we plot the experimentally determined values of SOC together with those predicted by the band-structure calculations. There is a clear correlation between the two data sets which gives evidence in favour of the correctness of our interpretation. We note that renormalization of SOC itself is not trivial and further theoretical studies are required to understand
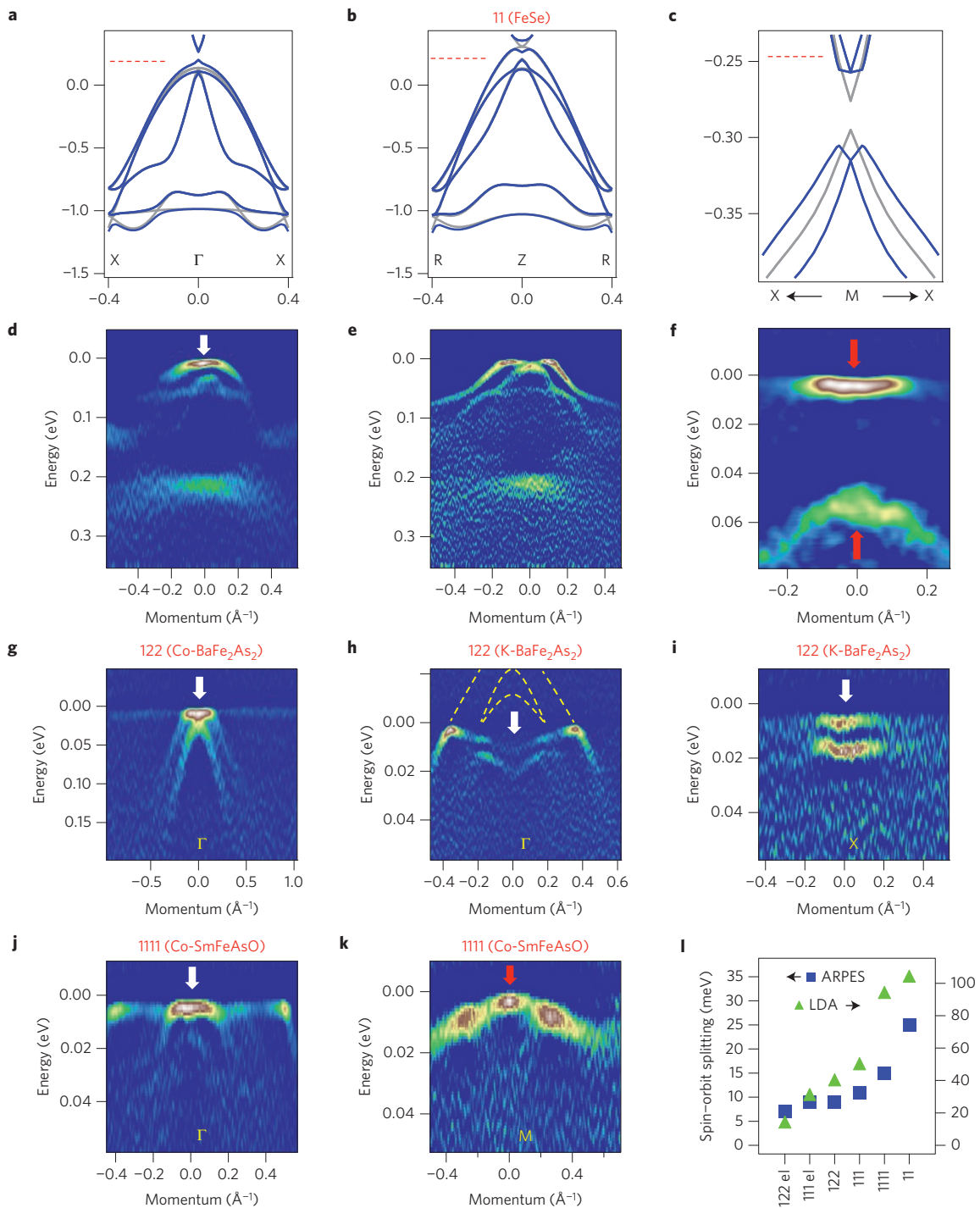
Figure 4 | Spin–orbit coupling in 11, 122 and 1111 iron-based superconductors. a–c, Results of the band-structure calculations of FeSe excluding SOC (grey lines) and including SOC (blue lines) along the high-symmetry directions. **d–f**, Corresponding experimental data, shown as second derivatives of the raw data. Note that in **c** two single features are observed at the M-point, contrary to the expected two double features in the nematic scenario. **g–i**, Same for 122 materials. Dashed lines in **h** show the expected dispersions in the unoccupied part of the spectrum. **j,k**, Same for Co-SmFeAsO. **l**, Comparison of the experimental values for SOC obtained by reading the peak positions from the corresponding EDCs shown in Supplementary Fig. 3, with the theoretical values. 'el' means electron pocket. Corresponding raw data are presented in Supplementary Fig. 2.

the mechanism of interplay between Hund's rule coupling and spin–orbit interaction.

The detection of SOC and the presence of the $3z^2 - r^2$ band at the Fermi level drastically change our knowledge of the low-energy electronic structure and Fermi surface in IBS in comparison with the initially considered nested circular FS with well-defined orbital character. Not only are the Fermi surfaces of all optimally doped

IBS formed by singularities in the centre and/or in the corners of the BZ (refs 14–17,21,22), but also their orbital composition becomes more complicated because of SOC-induced orbital mixing (see Supplementary Fig. 4).

We expect that these findings are highly relevant for the superconductivity in IBS. Existing approaches[18–20] strongly rely on the presence of shallow bands crossing the Fermi level with an
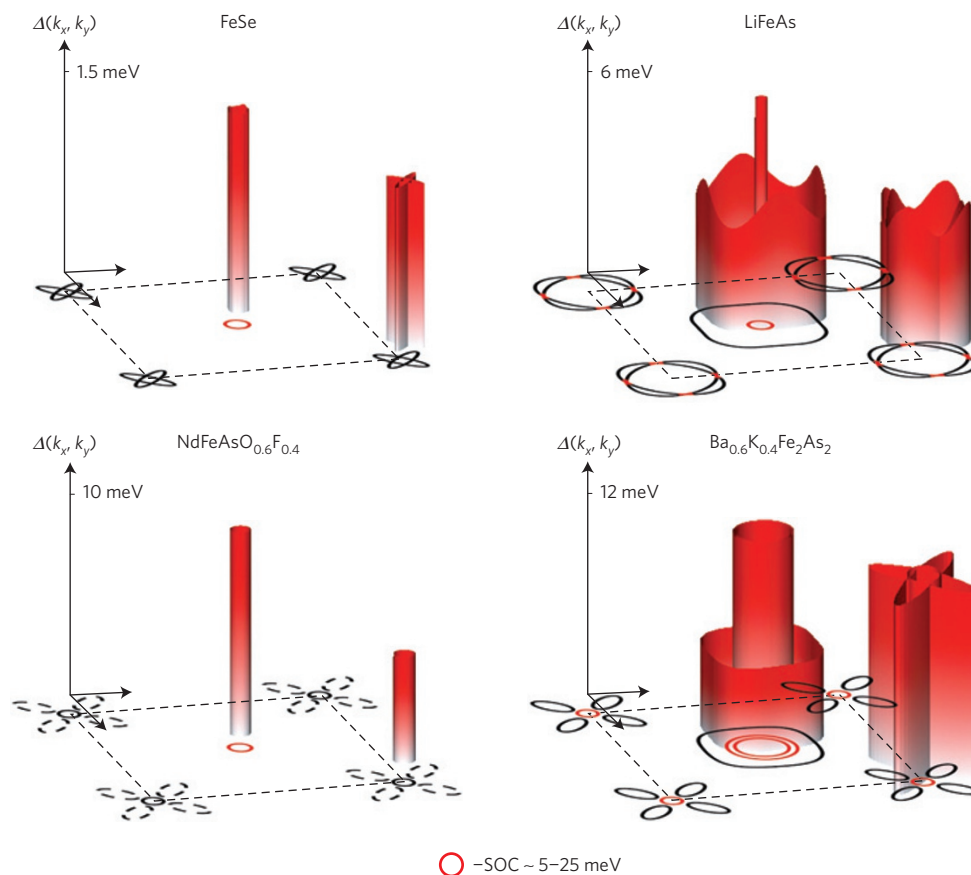
Figure 5 | Spin–orbit coupling and gap functions in iron-based superconductors. Sketches of the Fermi contours are shown in the horizontal plane. Fully red or partially red contours are the states at the Fermi level induced by the large (5–25 meV) spin–orbit splitting detected experimentally. Gap functions are given by the third axis and shown only for the centres and one of the corners of the BZ for simplicity. All gap functions are normalized to the maximum value indicated in each plot. The data for 111, 122 and 1111 IBS are taken, respectively, from refs 22,27 and (A. Charnukha et al., manuscript in preparation). Gaps in FeSe are determined in the present study and equal to 1.5 and 1.2 meV in the centre and corner of the BZ, respectively.

energy dispersion of the order of the pairing interaction. Another theoretical study demonstrates that the inclusion of SOC leads to further mixing of triplet pairing, as well as to an anisotropic energy gap on all Fermi surfaces in iron-based superconductors[26], the latter being observed experimentally[22]. In Fig. 5 we schematically show the Fermi surface contours and gap functions for the representatives of IBS families having the highest T_c. We mark in red those Fermi surfaces or their portions which are formed by the spin–orbit split states. Remarkably, the largest superconducting gap in each material is supported by the SOC-induced Fermi surfaces. Moreover, in 11 and 122 IBS, where the SOC in the corner of the BZ is comparable to that in the centre, one sees correspondingly considerable superconducting gaps.

We have thus observed the decisive influence of the spin–orbit interaction on the low-energy electron dynamics of all representative iron-based superconductors, which is much stronger than possible nematic effects. The size of SOC is comparable to the pairing gap and the Fermi energy, which may have profound implications on the mechanism of superconductivity in these materials.

Methods

Methods and any associated references are available in the online version of the paper.

References

1. Jungwirth, T., Wunderlich, J. & Olejník, K. Spin Hall effect devices. *Nature Mater.* **11,** 382–390 (2012).
2. Hasan, M. Z. & Kane, C. L. Topological insulators. *Rev. Mod. Phys.* **82,** 3045–3067 (2010).
3. Mourik, V. et al. Signatures of Majorana fermions in hybrid superconductor–semiconductor nanowire devices. *Science* **336,** 1003–1007 (2012).
4. Caviglia, A. D. et al. Tunable Rashba spin–orbit interaction at oxide interfaces. *Phys. Rev. Lett.* **104,** 126803 (2010).
5. Dikin, D. A. et al. Coexistence of superconductivity and ferromagnetism in two dimensions. *Phys. Rev. Lett.* **107,** 056802 (2011).
6. Gardner, H. J. et al. Enhancement of superconductivity by a parallel magnetic field in two-dimensional superconductors. *Nature Phys.* **7,** 895–900 (2011).
7. Haverkort, M. W. et al. Strong spin–orbit coupling effects on the Fermi surface of Sr_2RuO_4 and Sr_2RhO_4. *Phys. Rev. Lett.* **101,** 026406 (2008).
8. Kuroki, K. et al. Unconventional pairing originating from the disconnected Fermi surfaces of superconducting $LaFeAsO_{1-x}F_x$. *Phys. Rev. Lett.* **101,** 087004 (2008).
9. Hirschfeld, P., Korshunov, M. & Mazin, I. Gap symmetry and structure of Fe-based superconductors. *Rep. Prog. Phys.* **74,** 124508 (2011).
10. Kontani, H. & Onari, S. Orbital-fluctuation-mediated superconductivity in iron pnictides: Analysis of the five-orbital Hubbard–Holstein model. *Phys. Rev. Lett.* **104,** 157001 (2010).
11. Nakayama, K. et al. Reconstruction of band structure induced by electronic nematicity in an FeSe superconductor. *Phys. Rev. Lett.* **113,** 237001 (2014).
12. Shimojima, T. et al. Lifting of xz/yz orbital degeneracy at the structural transition in detwinned FeSe. *Phys. Rev. B* **90,** 121111 (2014).
13. Watson, M. D. et al. Emergence of the nematic electronic state in FeSe. *Phys. Rev. B* **91,** 155106 (2015).

14. Maletz, J. *et al.* Photoemission and muon spin relaxation spectroscopy of the iron-based $Rb_{0.77}Fe_{1.61}Se_2$ superconductor: Crucial role of the cigar-shaped Fermi surface. *Phys. Rev. B* **88,** 134501 (2013).
15. Thirupathaiah, S. *et al.* Why T_c of $(CaFeAs)_{10}Pt_{3.58}As_8$ is twice as high as $(CaFe_{0.95}Pt_{0.05}As)_{10}Pt_3As_8$. *Phys. Rev. B* **88,** 140505 (2013).
16. Maletz, J. *et al.* Unusual band renormalization in the simplest iron-based superconductor $FeSe_{1-x}$. *Phys. Rev. B* **89,** 220506(R) (2014).
17. Charnukha, A. *et al.* Interaction-induced singular Fermi surface in a high-temperature oxypnictide superconductor. *Sci. Rep.* **5,** 10392 (2015).
18. Innocenti, D. *et al.* Shape resonance for the anisotropic superconducting gaps near a Lifshitz transition: The effect of electron hopping between layers. *Supercond. Sci. Technol.* **24,** 015012 (2011).
19. Innocenti, D. *et al.* Resonant and crossover phenomena in a multiband superconductor: Tuning the chemical potential near a band edge. *Phys. Rev. B* **82,** 184528 (2010).
20. Bianconi, A. Quantum materials: Shape resonances in superstripes. *Nature Phys.* **9,** 536–537 (2013).
21. Borisenko, S. V. *et al.* Superconductivity without nesting in LiFeAs. *Phys. Rev. Lett.* **105,** 067002 (2010).
22. Borisenko, S. V. *et al.* One-sign order parameter in iron based superconductor. *Symmetry* **4,** 251–264 (2012).
23. Miao, H. *et al.* Coexistence of orbital degeneracy lifting and superconductivity in iron-based superconductors. *Phys. Rev. B* **89,** 220503(R) (2014).
24. Fernandes, R. M. & Vafek, O. Distinguishing spin–orbit coupling and nematic order in the electronic spectrum of iron-based superconductors. *Phys. Rev. B* **90,** 214514 (2014).
25. Evtushinsky, D. V. *et al.* Fusion of bogoliubons in $Ba_{1-x}K_xFe_2As_2$ and similarity of energy scales in high temperature superconductors. Preprint at http://arXiv.org/abs/1106.4584 (2011).
26. Cvetkovic, V. & Vafek, O. Space group symmetry, spin–orbit coupling, and the low-energy effective Hamiltonian for iron-based superconductors. *Phys. Rev. B* **88,** 134510 (2013).
27. Evtushinsky, D. V. *et al.* Strong electron pairing at the iron $3d_{xz,yz}$ orbitals in hole-doped $BaFe_2As_2$ superconductors revealed by angle-resolved photoemission spectroscopy. *Phys. Rev. B* **89,** 064514 (2014).

Acknowledgements

Author contributions

S.V.B., D.V.E., T.K.K., M.H. and Z.-H.L. performed ARPES experiments. A.N.Y. carried out band-structure calculations. I.M., R.K., S.W., B.B., T.W. and N.D.Z. provided high-quality single crystals. S.V.B. analysed the data and wrote the paper. All authors contributed to the preparation and revisions of the manuscript.

Additional information

Supplementary information is available in the online version of the paper. Reprints and permissions information is available online at www.nature.com/reprints. Correspondence and requests for materials should be addressed to S.V.B.

Competing financial interests

The authors declare no competing financial interests.

Methods

ARPES measurements were performed at the I05 beamline of the Diamond Light Source and at the 1^3-ARPES set-up of BESSY (HZB). Single-crystal samples were cleaved *in situ* at a pressure lower than 2×10^{-10} mbar and measured at temperatures ranging from 6 to 25 K ($\sim$1 K at BESSY). Measurements were performed using (s,p)-polarized synchrotron light from 18 to 120 eV and employing a Scienta R4000 hemispherical electron energy analyser with an angular resolution of 0.2°–0.5° and an energy resolution of 3–20 meV.

Band-structure calculations were performed for the experimental crystal structures (for example, ref. 28 for LiFeAs) in the local density approximation (LSDA) using the linear muffin-tin orbital (LMTO) method. Some details of the implementation of the PY LMTO code (A. Y. Perlov *et al.*, manuscript in preparation) can be found in ref. 29. Spin–orbit coupling was added to the LMTO Hamiltonian at the variational step. Because LiFeAs does not show magnetic order, ARPES spectra are compared to non-spin-polarized band structure, although LSDA calculations give a magnetic ground state with strip-like antiferromagnetic order and a slightly lower total energy.

LiFeAs single crystals in the form of packets of plates with dimensions of up to 1 cm were grown by self-flux using the standard method[30]. For the ARPES study single-crystal plates with dimensions of $3 \times 3 \times 0.1$ mm^3 have been selected.

High-quality single crystals of superconducting $SmFe_{0.92}Co_{0.08}AsO$ with lateral dimensions up to 0.3 mm were grown by the high-pressure high-temperature cubic anvil technique[31].

References

28. Pitcher, M. J. *et al.* Structure and superconductivity of LiFeAs. *Chem. Commun.* **101,** 5918–5920 (2008).
29. Antonov, V., Harmon, B. & Yaresko, A. *Electronic Structure and Magneto-Optical Properties of Solids* (Kluwer Academic Publishers, 2004).
30. Morozov, I. *et al.* Single crystal growth and characterization of superconducting LiFeAs. *Cryst. Growth Des.* **10,** 4428–4432 (2010).
31. Zhigadlo, N. D. *et al.* High-pressure flux growth, structure, and superconducting properties of LnFeAsO (Ln = Pr, Nd, Sm) single crystals. *Phys. Rev. B* **86,** 214509 (2012).